

# Overview of CFD Validation Experiments for Circulation Control Applications at NASA

G.S. Jones,<sup>1</sup> J.C. Lin\*, B.G. Allan\*, W.E. Milholen,<sup>2</sup> C.L. Rumsey,<sup>†</sup> R.C. Swanson<sup>†</sup>  
NASA Langley Research Center, Hampton, Virginia, 23681

Circulation control is a viable active flow control approach that can be used to meet the NASA Subsonic Fixed Wing project's Cruise Efficient Short Take Off and Landing goals. Currently, circulation control systems are primarily designed using empirical methods. However, large uncertainty in our ability to predict circulation control performance has led to the development of advanced CFD methods. This paper provides an overview of a systematic approach to developing CFD tools for basic and advanced circulation control applications. This four-step approach includes "Unit", "Benchmark", "Subsystem", and "Complete System" experiments. The paper emphasizes the ongoing and planned 2-D and 3-D physics orientated experiments with corresponding CFD efforts. Sample data are used to highlight the challenges involved in conducting circulation control computations and experiments.

## Nomenclature

AOA	= angle of attack (degrees)	w	= slot width (inches)
AR	= aspect ratio	X	= streamwise tunnel coordinate (inches)
b	= span (inches)	Y	= horizontal cross plane tunnel coordinate (inches)
CC	= circulation control	Z	= vertical cross plane tunnel coordinate (inches)
$C_p$	= pressure coefficient		
$C_D$	= drag coefficient	<b>Symbols:</b>	
$C_d$	= section drag coefficient	$\alpha$	= pitch angle of attack (deg)
$C_L$	= lift coefficient	$\delta$	= jet angle relative to free stream (deg)
$C_l$	= section lift coefficient	$\delta^*$	= boundary layer displacement thickness
$C_\mu$	= momentum coefficient	$\gamma$	= ratio of specific heats
C, c	= chord, wing, airfoil (inches)	$\rho$	= density
h	= slot height (inches)	$\phi$	= separation angle relative to model (deg)
LE	= leading-edge	$\Gamma$	= circulation
TE	= trailing-edge	$\theta$	= separation angle relative to free stream (deg)
MAC	= mean aerodynamic chord (inches)		
M	= Mach number	<b>Subscripts</b>	
m	= mass flow rate (lbm/sec)	J	= jet
NPR	= nozzle pressure ratio	o	= free stream total condition
P	= pressure (psf)	$\infty$	= free stream static condition
q	= dynamic pressure (psf)		
r	= radius of Coanda surface or flap (inches)		
Re	= Reynolds number		
R	= gas constant		
S	= planform area (in <sup>2</sup> )		
T	= temperature (°F)		
U	= velocity component in streamwise direction (ft/sec)		
V	= velocity component in horizontal cross plane (ft/sec)		
W	= velocity component in vertical cross plane (ft/sec)		

<sup>1</sup> Researcher, Ph.D., Flow Physics and Control Branch

<sup>2</sup> Researcher, Ph.D., Configuration Aerodynamics Branch

<sup>†</sup> Researcher, Ph.D., Computational AeroSciences Branch

## Introduction

Recent interest in circulation control (CC) technology has been prompted by the National Aeronautic and Space Administration (NASA) Cruise Efficient Short Take Off and Landing (CESTOL) initiative and the Air Force Research Laboratory (AFRL) Advanced Joint Air Combat System program. These initiatives highlight the need for improved high-lift or powered-lift systems to meet takeoff and landing goals that are integrated into transonic cruise configurations. Because circulation control technology will require significant modifications to the aircraft design it will need to “buy” its way onto the aircraft. This will require designers to optimize the entire wing and propulsion system with particular attention on air delivery system efficiency, safety concerns related to an engine out condition, and control issues related to large aerodynamic moments.

The rapid turnaround required by designers to complete trade studies normally limits the use of Computation Fluid Dynamic (CFD) tools to the improvement of empirical methods. Empirical methods derived from experiments are traditionally used in the design process. However, the complexities of many flow control techniques in use today, including circulation control, far exceed the experimental databases used to develop the empirical methods. By coupling physics-based CFD tools with validation experiments we can develop parametric studies that characterize the sensitivities of wing geometries and blowing systems, required to advance empirical techniques necessary to design a CESTOL type aircraft.

The application of the state of the art CFD tools to a CC airfoil with an experimental database was described at the 2004 NASA/ONR Circulation Control workshop.<sup>i</sup> Results from that workshop showed that CFD simulations were unable to consistently and accurately predict the performance of a CC airfoil. An example of one of the CFD predictions is shown in Figure 1. The failure to match the jet separation and the streamline turning for this example was linked to turbulence models<sup>ii,iii</sup> and CFD grid issues. In addition to identifying inconsistencies in CFD prediction capability, the workshop also identified that the experimental databases were inadequate for CFD validation.

This paper describes a systematic approach to developing experimental and computational databases for improving CC prediction capability. In general, CFD validation is defined by determining how well the CFD model predicts the performance and flow physics when used for its intended purposes.<sup>iv</sup> The level of CFD validation can be defined by the complexity of the code and the experiment being used for validation, as described in Figure 2.<sup>v</sup> These levels of validation are being pursued using NASA’s airfoil, semi-span wing, and full-span Hybrid Wing Body geometries that are the focus of this paper.

For the purposes of this paper the term circulation control implies using a tangential jet on a highly curved aerodynamic or Coanda surface. The aerodynamic characteristics of circulation control wings have been experimentally and numerically studied since Henri Coanda’s near fatal crash in 1910<sup>vi,vii,viii</sup> Many of these studies have concentrated on the lift performance related to trailing edge shape, slot height, and blowing rates. Despite the large potential performance improvements related to circulation control, only two fixed wing flight demonstrations<sup>ix,x,xi</sup> have been evaluated. The results of both demonstrator programs showed large benefits of circulation control applications for short runways. Without requirements for short runway access, however, circulation control applications were not pursued and the remaining work was largely a laboratory effort.

The renewed interest in CESTOL aircraft at NASA has been prompted by the escalating airport congestion and noise abatement criteria.<sup>xii,xiii</sup> The FAA<sup>xiv</sup> has projected that air traffic will increase by a factor of 2 or more within the next 20 years. Airport noise has been identified by the FAA as the largest problem for 50 of the nation’s airports.<sup>xv</sup> One way to alleviate these problems is to use the shorter runways and the infrastructure that are already in existence at under utilized small airports.<sup>xvi,xvii</sup> It may also be necessary to alter the traffic patterns and glide slopes to keep the noise confined to the airport boundaries.<sup>xviii,xix</sup> These issues have prompted engineers at NASA to evaluate the improvements in aircraft take off and landing capabilities that can be integrated into efficient cruise geometries.

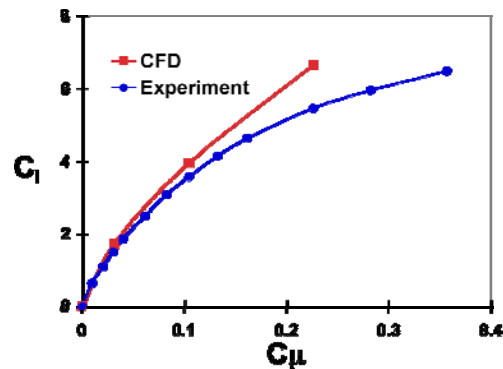


Figure 1. Comparison of experimental and Reynolds Average Navier Stokes (RANS) CFD lift performance data for a typical CC airfoil

NASA has set goals<sup>xx,xxi</sup> for a state-of-the-art 100 passenger airliner to be operational by the year 2022 and to have the following characteristics:

- take-off and landing distance of less than 2,000 feet,
- cruise Mach number  $\geq 0.8$ ,
- 1,400 to 2,000 mile range capability,
- noise containment within an airport footprint, and
- low speed maneuverability

Improvement and optimization of advanced flow control systems and wing geometries are required to achieve these goals. Several advanced flow control and propulsion technologies are being considered to meet these goals, including CC, upper surface blowing, over the wing vectored blowing and/or combinations of these technologies. To achieve an optimized CESTOL geometry, it is necessary to evaluate the requirements of the aircraft.<sup>xxii,xxiii</sup> These current CESTOL goals are being continually influenced and refined by issues such as fuel prices and new air traffic requirements. However, pursuing these goals using CC may provide a low speed performance capability that exceeds what can be achieved with conventional high lift systems. In the remainder of the text we will discuss the use and validation of CFD for advanced CESTOL type of aircraft.

### Code Validation Process for Circulation Control

Circulation control applications are difficult to compute reliably using state-of-the-art CFD methods as demonstrated by the inconsistencies in CFD prediction capability described in the 2004 NASA/ONR Circulation Control workshop.<sup>1</sup> For Reynolds-averaged Navier-Stokes methods, some turbulence models such as Menter SST k- $\omega$ <sup>xxiv</sup> and Spalart-Allmaras with rotation and curvature correction (SARC)<sup>xxv</sup> have been shown to predict CC flows reasonably well only at certain conditions while other methods have been shown to be very sensitive to numerical parameters. There is also a tendency for the predictive capability of CFD to degrade as the blowing increases. While it is possible that turbulence models bear

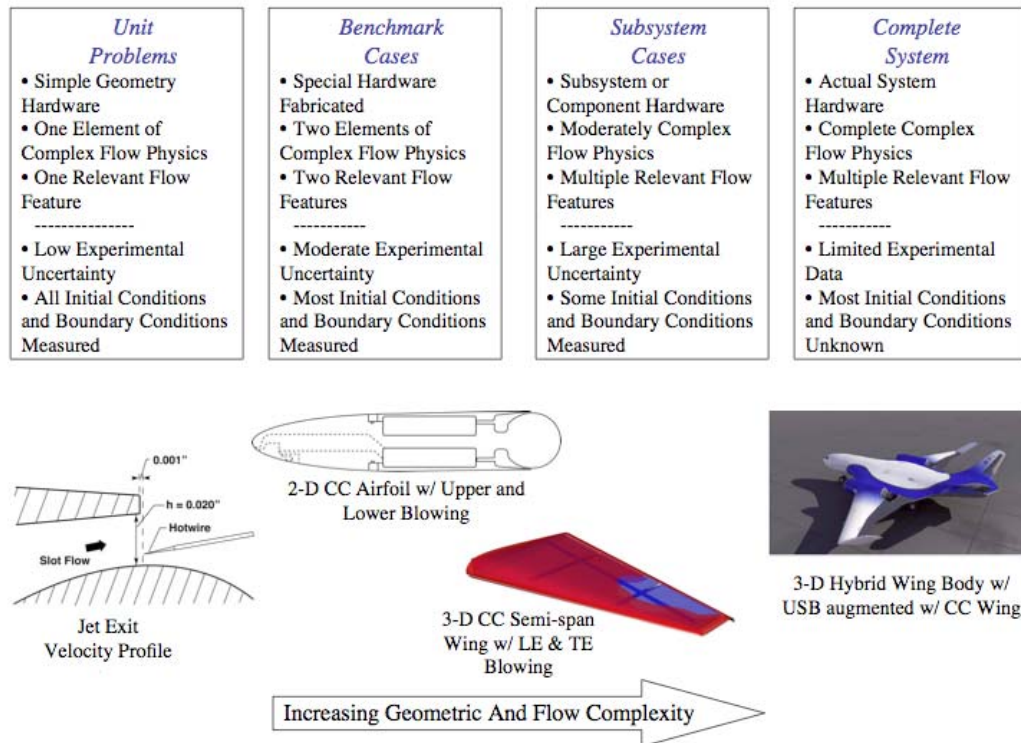
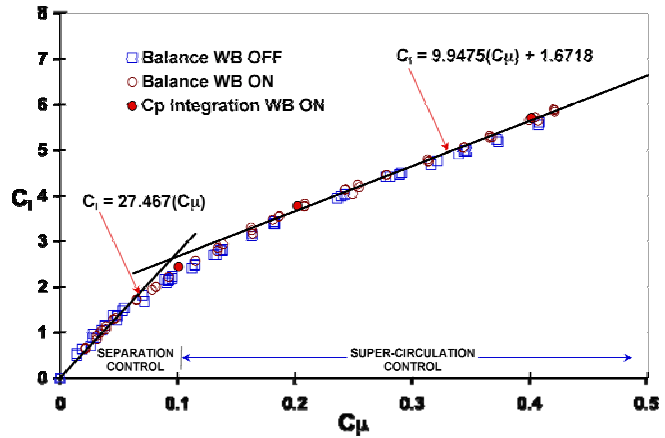


Figure 2. Four levels of CFD validation used to study circulation control

some responsibility, some of the disagreement may be due to an increasing loss of two-dimensionality in nominally 2-D experiments as the blowing rates increase. Unfortunately, it is difficult to determine the sources of the discrepancies because most of the CC experiments have not been adequately documented for CFD validation.

One of the parameters that CC performance is typically characterized by and that must be carefully documented is the thrust or momentum coefficient,  $C_{\mu}$ . The sensitivity of the airfoil performance to  $C_{\mu}$  is dependent on the jet characteristics and the airfoil geometry,<sup>xxvi</sup> particularly on the surface near the jet exit. There are two physical regimes that define circulation control as a function of blowing.<sup>xxvii</sup> These regimes are commonly referred to as *separation control* and *super-circulation control* and exhibit different global efficiencies as determined by the change in unit lift due to the change in unit blowing as shown by the data in Figure 3.



**Figure 3. Circulation control flow regimes showing sensitivities and influence of wall blowing (WB)**

The physical description of the efficiencies of these regimes is demonstrated by the relationship of the jet separation location on the trailing edge surface and the interaction of the jet with the on-coming flow. Nominally the flow separation on the flap or Coanda surface is a function of the pressure gradient along the surface. As the thin jet is applied, the flow separation is moved aft along the surface. This jet also entrains and accelerates the flow in the vicinity of the wall-bounded jet, thus increasing the turning of the streamlines near the trailing edge. This also affects the leading edge stagnation region thus increasing the overall circulation around the airfoil and the lift.

The transition from one regime to another is not always clearly identified and is dependent on the sharpness of the trailing edge. The systematic study of this mechanism should include different trailing edge geometries that include a hinged flapped geometry (i.e. fixed separation located at tip of flap) and a circular geometry (i.e. separation location free to move up to 180°) as shown in Figure 4.

NASA’s approach to resolve the issues of CFD inconsistency and the inability to match experiments at high-blowing conditions involves a strong interaction between CFD and experimental investigations. For CFD it is believed that most of the challenges exist in establishing consistent requirements for boundary conditions, along with guidelines for numerical methodology, such as the use of sufficient grid refinement as well as transition and other parameters that can influence the solution. The planned development of CFD tools for circulation control applications utilizes RANS and LES codes. The benefits of understanding the physics of complex flow fields to improve the prediction and modeling techniques in CFD codes should also be used to improve appropriate experimental methods.

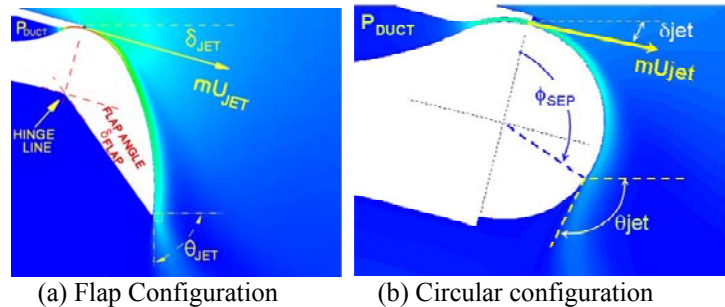


**Figure 4. Example of two Coanda surfaces.**

The goal of this series of investigations is to acquire error bounded experimental results suitable for CFD validation with no attempt to achieve maximum performance on a specific geometry. The approach for these experiments is to develop a 2-D fundamental circulation control database that will be followed by a 3-D database that captures realistic physics to advance predictive tool development.

An often-overlooked aspect of the quality of information from CC experiments pertains to the quantification of the blowing parameters. An example of this is quickly shown by considering the methods used to determine  $C_{\mu}$ . The momentum coefficient can be determined by the quantities shown in either Equation 1 or 2. Equation 1 expresses the momentum coefficient in terms of basic geometric and flow parameters. For small-scale experiments, the uncertainty of the slot height ( $h$ ) dominates Equation 1, because the absolute slot height measurement error (e.g.  $\pm 0.002''$ ) is typically large relative to the total slot height. This measurement can also be complicated by non-uniformities in the slot along the airfoil span and by small changes in slot height when the internal duct is pressurized. Using Equation 2 simplifies the required measurements for determining  $C_{\mu}$  by eliminating the need to measure slot geometry or jet density. These parameters are integrated into the mass flow rate, which can be measured directly. An additional common error is in the calculation of the jet velocity,  $U_j$ . A commonly accepted method for calculating the jet velocity assumes that the jet flow expands isentropically to the freestream static pressure as shown in Equation 3. This introduces an error since the static pressure at the jet exit is less than the freestream static pressure (as demonstrated in surface pressure measurements) at the jet exit. When Equation 1 is used, the error is exacerbated since the  $U_j$  value is squared. While the momentum uncertainties are typically smaller when using Equation 2, it is often a CFD validation requirement that the individual parameters be measured. The uncertainties for these parameters are cumulative and are dependent on the transducers and the instrumentation used for the measurement.<sup>xxviii,xxix</sup> It is recommended that multiple measurement techniques be used to quantify these uncertainties.

$$C_{\mu} = \frac{\text{THRUST}}{q_{\infty} S} = \frac{2hb_{\text{JET}}}{cb} \frac{\rho_{\text{JET}}}{\rho_{\infty}} \frac{U_{\text{JET}}^2}{U_{\infty}^2} \quad (1)$$

$$C_{\mu} = \frac{\text{THRUST}}{q_{\infty} S} = \frac{m U_{\text{JET}}}{q_{\infty} S} \quad (2)$$

Where,

$$U_{\text{JET}} = \sqrt{\frac{2\gamma b_{\text{JET}} (T_{0\text{JET}})}{\gamma - 1} \left(1 - \frac{P_{\infty}}{P_{0\text{JET}}}\right)^{\frac{\gamma - 1}{\gamma}}} \quad (3)$$

and

$$\dot{m} = \rho_{\text{JET}} U_{\text{JET}} (h)(w) \quad (4)$$

## Description of Validation Cases

In this section, we will provide a description of the experiments in terms of the systematic approach shown in Figure 2. Example experimental and CFD results will emphasize the critical features related to circulation control physics.

### Unit Problem

One of the main factors influencing the CFD solution is the characterization of the wall jet at the jet exit. This can be set with a boundary condition of specified velocity or momentum either at the jet exit plane, or at an inner plenum wall. In the latter case, the flow (including turbulence) is allowed to adjust naturally as it is forced out of the high-pressure plenum. An example showing the complexity of the results from a computation that includes a plenum is shown in Figure 5. In the former case, it is more difficult to prescribe realistic profiles at the exit plane. Unfortunately, both methods have traditionally relied upon under-resolved details from the experiment. The only information available from experiments regarding the jet has often been the jet momentum coefficient,  $C_{\mu}$ , as determined by Equation (1). In this equation, the jet velocity is typically obtained from conditions inside the plenum, combined with isentropic flow relations. This methodology introduces additional uncertainty into the CFD simulation. Measurements of flow conditions, especially the velocity at the jet exit, help

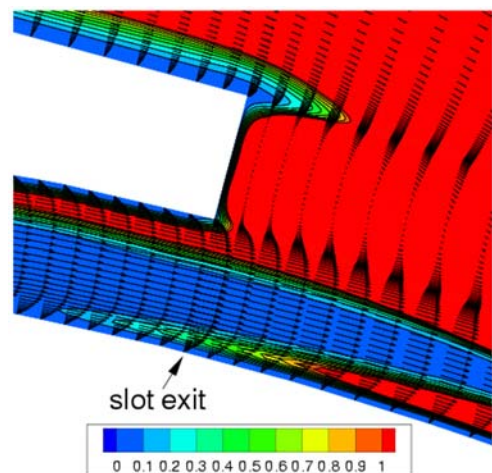
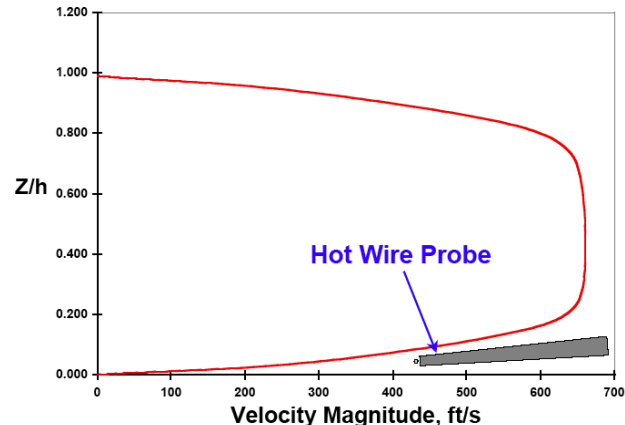


Figure 5. Flow near the upper-surface blowing slot of an airfoil, showing normalized turbulent viscosity contours along with mean flow velocity vectors (the plenum is to the left of the lower channel)

to remove this uncertainty by establishing definitive boundary conditions to match at and near the jet exit.

Implementation details of the CFD boundary condition at the plenum inflow are probably not too important, as long as the plenum is of sufficient size and provides the desired momentum flux. For many studies, the velocity and density (i.e., momentum) are specified at the upstream face inside the plenum, and the pressure is extrapolated from the interior of the domain. Other internal plenum boundary conditions were also tried by the authors, such as specifying total pressure along with total temperature (and extrapolated pressure), but it made little difference to the solution.

The small size of the jet slot height often complicates measurement of the jet profile. For small scale wind tunnel experiments, the slot height can range from  $0.010'' < h < 0.60''$ . A nominal slot height of  $0.020''$  is typical of geometries described in this paper. Miniature pitot probes have an outer diameter of  $0.010''$  resulting in a large bias due to integration in the large velocity gradients typical of wall bounded jets. The use of hot wire probes does not come without measurement difficulties that include interpretation of transonic hot wire results. The hot wire prongs can be as large as 5% to 10% of the slot height as shown in figure 6. This is often complicated by model and probe vibration. All of these factors lead to measurement uncertainties that must be quantified.



**Figure 6. CFD velocity profile at the jet exit with scaled hot wire probe,  $C_{\mu}=0.119$ ,  $NPR=1.2$ ,  $h=0.020''$**

Another relevant factor related to the jet exit flow is the oncoming boundary layer above the lip of the slot. Because this boundary layer interacts/mixes with the jet, it is important that it be characterized correctly in the CFD solution. Accurate experimental measurements of boundary layer profiles and turbulence properties in this region are needed for validation.

## Benchmark Cases

Two benchmark cases will be described as part of the systematic CC validation effort. Two of the desired features for each of the benchmark CFD validation studies are a simple geometry that is capable of super-circulation and measured critical boundary conditions required by modern CFD codes. Even though the geometries are simple, a 2-D lift coefficient of 7 – 8 can be achieved in the super-circulation regime.

### *The 2-D Benchmark case*

Two-dimensional CFD has proven itself to be useful for many aerospace design and trade studies. However, when validating turbulence models for specific new applications, it is extremely important to ensure that consistent conditions (geometry and boundary) are being considered for the computation and the experiment. For CC airfoils, this can be difficult to ascertain because of the sensitivity of the Coanda surface flow separation to jet boundary conditions and other factors that can be problematic to measure, as well as the inherent difficulty of maintaining two-dimensionality in the experiment at high blowing conditions. In ongoing work at NASA we are attempting to address these issues, with the ultimate goal of validating the capabilities of existing turbulence models for 2-D CC flows over a wide range of blowing conditions.

To reduce uncertainty and to optimize the measurement capability, two independent wind-tunnel tests were conducted using the same model. The NASA LaRC Basic Aerodynamic Research Tunnel (BART) and the Georgia Tech Research Institute's Model Test Facility (MTF) are comparable in size and speed, but emphasize different measurement techniques. The BART test series emphasizes the external flow physics by identifying the leading edge stagnation point, determining the jet separation location, and determining the jet trajectory for selected blowing conditions. The MTF test series characterizes the CC model's high-lift blowing performance as a function of slot height, angle of attack, and  $C_{\mu}$ .

A 2-D geometry with an elliptic leading edge and a large circular trailing edge profile, shown in Figure 7, was selected for the 2-D validation experiment. This geometry was chosen as the benchmark geometry for NASA's 2-D effort because it is characteristically simple and has a large trailing-edge radius for accurate measurements of jet separation. The dual blowing (both upper and lower surfaces) capability will be used to manage the drag characteristics, but will have a lower priority in the initial validation database experiments.

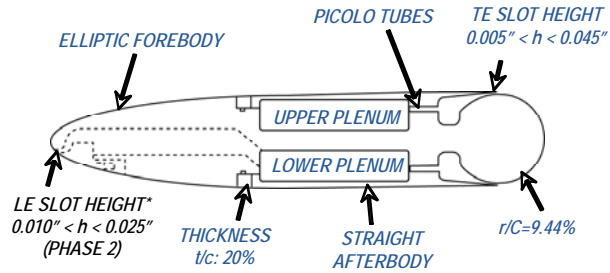


**Figure 7. NASA/GTRI 2-D CFD Validation Model, CC-E0020EJ airfoil**

While it has been difficult to compute 2-D circulation control applications reliably, it has also been difficult to generate 2-D experimental data independent of the influences from wind tunnel walls. The two-dimensionality of the flow and the wall effects are proportional to the amount of circulation control or lift generated by the wind tunnel model. The comparison made in Figure 1 between the two-dimensional CFD simulations and the wind tunnel measurements show how CFD tends to over predict the performance of a circulation control model at high lift coefficients where tunnel wall effects become large. These effects are generally related to the walls limiting the streamline turning, as shown in Figure 8, and the wall and model juncture for 2-D testing shown in Figure 9.

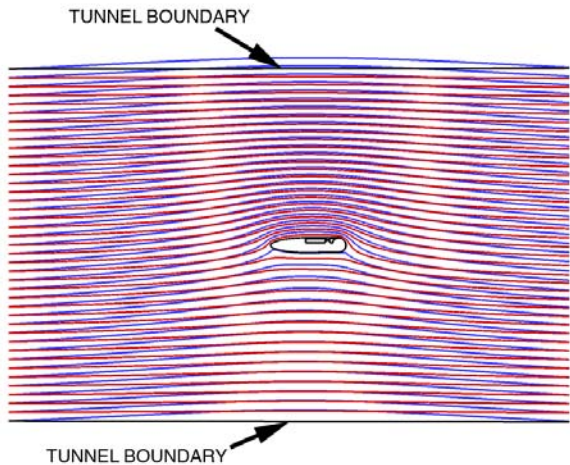


**Figure 8. 2-D CFD prediction of the floor and ceiling walls, AR=3.26,  $C_{\mu}$ =0.115, NPR=1.2  $C_l$ =4.87 (no walls, blue),  $C_l$ =4.43 (walls present, red),  $h/C$ =0.0023, wind tunnel height to chord=4.88, CC-E0020EJ airfoil**

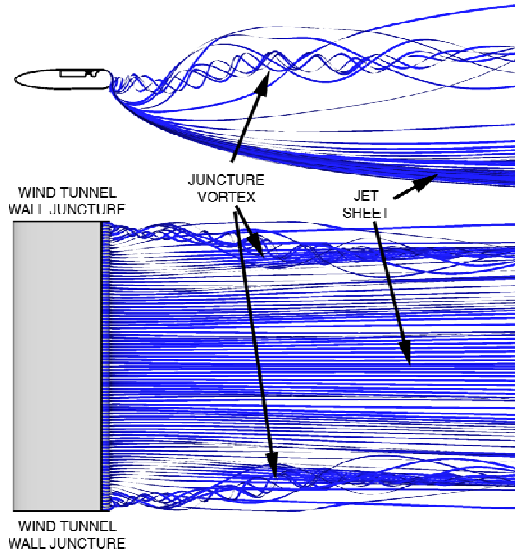


**Figure 9. 3-D CFD prediction of the wall juncture flow, AR=3.26,  $C_{\mu}$ =0.23, NPR=1.4  $C_l$ =5.09,  $h/C$ =0.0023, CC-E0020EJ airfoil**

The effect of the wind tunnel walls in the 2-D plane can be estimated by comparing the performance results with and without floor and ceiling walls. The presence of the walls decreased the lift coefficient by approximately 10% compared to free air calculations for the case shown in Figure 8. Three dimensional effects due to interactions with the spanwise walls are difficult to characterize in 2-D experiments. In similar experiments e.g., Novak et al.,<sup>xxx</sup> the interaction of the sidewall boundary layers with the wing and its Coanda jet produced vortical structures that induced downwash along the span of the wing, yielding relatively large recommended angle-of-attack corrections (e.g.,  $\Delta\alpha = -8.94$  deg for  $C_{\mu} = 0.226$ ). Estimated corrections such as this are necessary when comparing to 2-D CFD computations. If sidewall blowing or other sidewall boundary layer control is used, it is helpful to quantify its influence on the flowfield at various blowing rates.

An example of the Particle Image Velocimetry (PIV) data compared to 2-D RANS calculations, shown in Figure 10, illustrates how CFD can be used to estimate the AOA effects of the wind tunnel walls. The leading-edge stagnation location measured with the PIV data is at  $x/c$  value of 4.03%. The comparable CFD calculation in free air (i.e. no wind tunnel walls) identifies the stagnation to be at an  $x/c$  of 7.75%. An AOA adjustment of  $-5^\circ$  for the CFD simulation resulted in a close match to the experimental results for both the stagnation location and airfoil pressure distribution. The AOA adjustment based on classic wall corrections to account for tunnel wall interference is of this magnitude. Further investigation of wall interference using CFD tools is warranted.

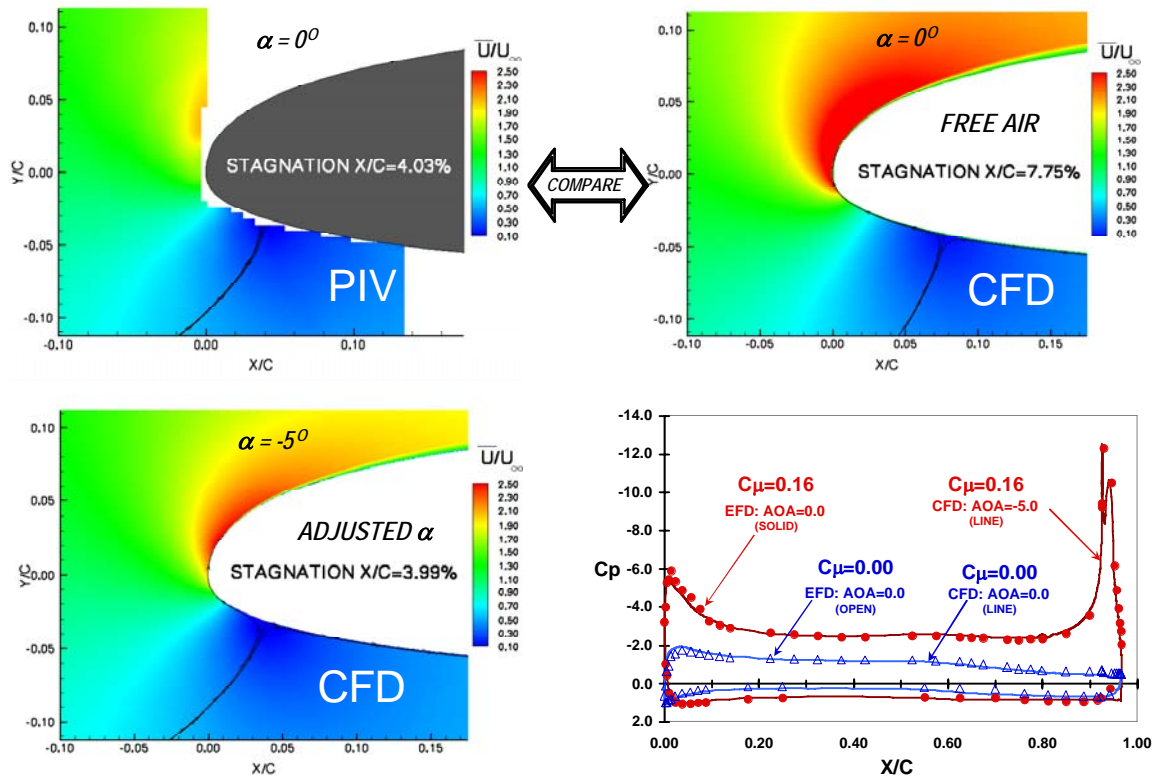


**Figure 10.** Example of PIV stagnation streamline data compared to CFD computations, GACC airfoil at  $\alpha_{\text{GEOMETRIC}} = 0^\circ$

The measurements of the external flow field are driven by two CFD validation requirements, (1) capture the global streamline behavior related to blowing, and (2) measure the boundary layer and jet characteristics on the airfoil. The measurement suite for this series of tests was driven by model scale and optical access. External flow measurements will be obtained using a 2-D PIV

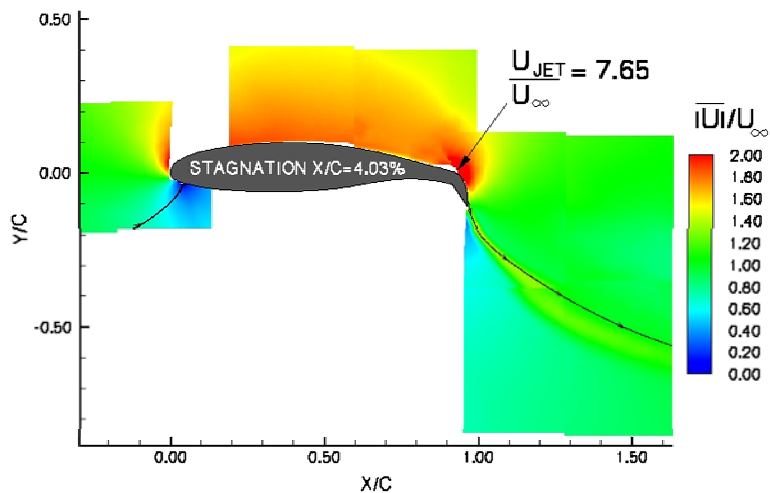


**Figure 11.** Example PIV data for GACC airfoil at  $\alpha_{\text{GEOMETRIC}} = 0^\circ$

system. This system will capture the details of the external flow to include the edge of the boundary layer. PIV measurements near the surface are problematic at this scale. Boundary layer details have been measured using a single-sensor hot wire. Examples of PIV measurements for a similar experiment are shown in Figure 11.

The boundary layer transition characteristics for low-Reynolds number testing are often difficult to assess. For this series of experiments, the tunnel velocity was increased until constant baseline drag was achieved. Based on this criteria, a minimal tunnel operational limit was established for the validation experiments of  $q=15$  psf, corresponding to  $Re_c=0.50 \times 10^6$ . Due to the presence of a laminar separation bubble near the leading edge of the model, a transition strip was added to the lower surface at  $x/c=3\%$ . Example pressure distributions are shown in Figure 12.

Because accurate computations of the jet are crucial, it is particularly important to measure the as-built slot width as a function of span to ensure adherence to specifications and minimal spanwise variation. Based on experience, the degree to which the slot geometry changes under pressure should be determined. In terms of boundary conditions, the jet conditions need to be measured as well as the freestream conditions at some specified location upstream in the wind tunnel.

In terms of the desired measurements for CFD validation, surface pressures (including spanwise variations) are necessary, along with integrated force and moment data. Boundary-layer/jet-velocity and turbulent shear stress profiles are the most useful quantities for judging the capabilities of the turbulence models. Without these measurements, it is difficult to make assessments because sometimes CFD values agree reasonably well with experimental surface pressures for the wrong reasons. In addition, the measured boundary-layer profiles on the airfoil upstream of the jet slot are extremely important to make sure that the “external” flow interacting with the jet is the correct one. Accurate measurements of the jet separation location off the Coanda surface as well as the stagnation streamline location near the leading edge are also key measures used to qualify the success of a CFD simulation. Imaging in the far-field away from walls can be useful, but it is not as important for the CFD validation as the other quantities listed above.

Characterization of the boundary layers (including jet) is generally needed at Reynolds numbers typical of most of the wind tunnel tests. In other words, where do the boundary layers and jet become turbulent? Is there a laminar bubble present on the airfoil? Is the jet issuing from the slot laminar, turbulent, or transitional?

### ***Semi-span Benchmark Experiments***

The primary objective of this experiment is to evaluate Reynolds number effects for advanced 3-D circulation control wings for both high-lift and cruise configurations using the same model. This unique data set will also provide a benchmark database for CFD validation. Many of the issues described for the 2-D benchmark validation experiment are still applicable for the semi-span experiment. These benchmark tests are being planned for the NASA LaRC National Transonic Facility (NTF) and the NASA LaRC 14-by-22-Foot Subsonic Tunnel to begin in the summer of 2009.

The design criteria for this series of experiments is based on a realistic cruise configuration that contains the blowing capability for circulation control powered lift and cruise enhancement. To be consistent with NASA CESTOL system studies<sup>xxxi</sup> a swept wing with an aspect ratio of 9.5 is desired. However, achieving this aspect ratio for the NTF semi-span study would require scaling the slot to unreasonably small values. The compromise was to design the outboard section of the wing for NTF (AR~5) and extend the wing to hybrid wing configuration for future low-speed testing in the LaRC 14-by-22-Foot Subsonic Tunnel and high-speed testing at NASA Ames Research Center’s 11-Foot Pressure Tunnel.

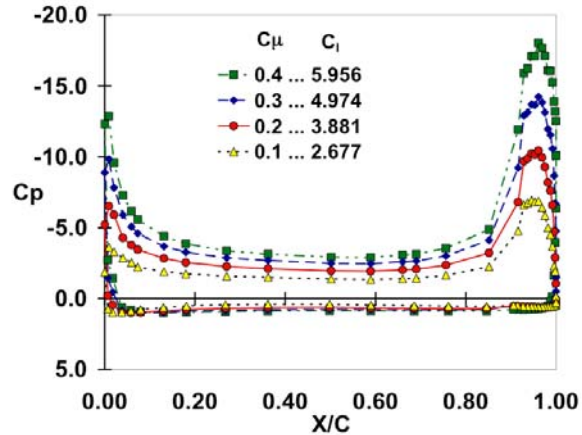


**Figure 12. Experimental pressure distributions and corresponding lift for the CC-E0020EJ**

While the goals of this semi-span CFD validation study are not intended to optimize wing geometry, it is desired to choose a state-of-the-art geometry with characteristics that are consistent with the CESTOL goals. Selection of the wing profile was therefore driven by the cruise performance (Mach > 0.8), thus limiting the trailing edge geometry to internally blown flaps.

The NASA TMA-0712 supercritical profile selected for the 3-D validation experiments will be modified to accommodate an upper-surface blowing slot that will be located at the break line of the trailing edge hinged flap shown in Figure 13. This wing will be fabricated using a modular approach. The model will have a removable trailing edge hinged flap and a removable leading edge that can accommodate leading edge blowing or variations with and without slats, or droop, etc. It is intended that the wing can be used for other approaches to active flow control for future development as well.

The NTF test will take advantage of cryogenic and pressure capabilities to achieve high Reynolds number conditions. Projected tunnel conditions will be limited to  $-50^{\circ}\text{F}$  and 5 atmospheres, resulting in a  $Re_c = 15 \times 10^6$  at Mach=0.2 and  $Re_c = 30 \times 10^6$  at Mach=0.8. The air delivery system for NTF is being developed for advanced blowing concepts that include 3-D circulation control. Volumetric flows must be controlled for a wide range of  $C_{\mu}$ 's, as shown in a typical operational map in Figure 14. A  $C_{\mu}$  or NPR sweep would typically operate at an average slot height, e.g.,  $h=0.060$  average shown with red line in Figure 14. The maximum jet flow condition will be limited to a jet mach number of 1. The air delivery and mass flow systems must be capable of low flow and high flow operations. These conditions typically require a dual flow control system that includes temperature control.

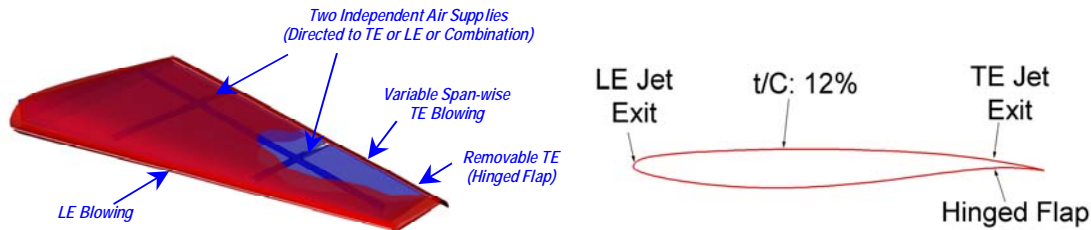


Figure 13. Sketch of NTF circulation control semi-span TMA-0712 model

The conceptual design of the semi-span circulation control model has dual flow paths for independent control of the two air delivery systems. Internal pressure vessels are being designed to be consistent with the circulation control operational requirements described above. Model design and fabrication are being performed in parallel with the development of the new NTF air delivery system. Initial testing is planned for the 3rd quarter of 2009.

The CFD modeling challenges discussed in the 2-D CFD development are noticeably increased for even a simplistic three-dimensional configuration such as that proposed for the NTF experiments. The increased flow field complexity is not the only pacing item, the growth in the grid complexity and density required to properly model the internal flow passages is another significant factor. Due to wind tunnel model size constraints and typically high plenum operating pressures, internal support structures are often required to maintain model integrity and geometric accuracy. Thus, a realistic CFD simulation requires adequate resolution of not only the support geometries, but also any anticipated induced flow features such as juncture vortices, or even localized flow separation. At a minimum, the support structures will influence the slot exit flow quantities and may well dominate the

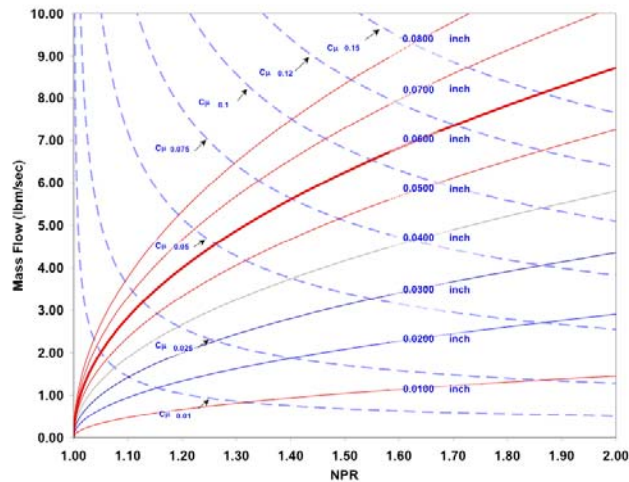
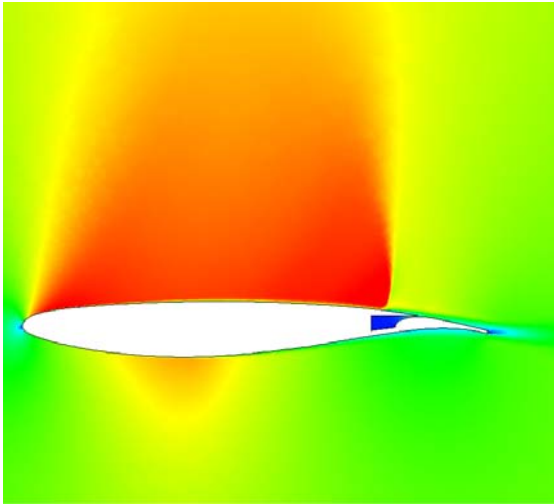


Figure 14. NTF air station operational requirements of model blowing system for different slot heights,  $T_o = -50^{\circ}\text{F}$ ,  $MAC = 17.4^{\circ}$ ,  $b = 44^{\circ}$ ,  $b_{\text{SLOT}}/b = 97.7\%$ ,  $P_o = 5 \text{ atm}$ ,  $M = 0.2$ .

internal flow field. Thus, documentation of the slot exit properties across the entire span of the wind tunnel becomes crucial.

The importance of documenting the approaching upper surface boundary layer was also discussed in the 2-D CFD section, but will be expanded upon in the context of adding cross flow, due to either wing sweep or leading edge flow separations. Depending on the location and orientation of the blowing slot, it is possible that a highly three-dimensional mixing and entrainment process will occur just downstream of the blowing slot. In some applications, this may be the desired effect, but will only complicate off-body flow-field measurements necessary for proper CFD code validation. Also, the addition of flap side-edge and wing-tip vortices further complicate the flow structure near the model. Obtaining accurate experimental measurements for these types of flows will be a taxing exercise for state-of-the-art measurement techniques, and it will likely require several techniques to be used in concert to achieve quantifiable uncertainties.

The following CFD examples highlight the unstructured flow solver USM3D being used to examine the effects of blowing at transonic and low-speed conditions. Representative Mach number contours shown in Figure 15 are for the modified NASA TMA-0712 airfoil. The Mach number is 0.78, the lift coefficient is 0.70, and NPR=1.25. The upper surface normal shockwave is just upstream of the blowing slot exit, and the blowing has been found to be effective in reducing the drag by reducing separation near the trailing edge of the airfoil. It should be noted that for the 3-D semispan model, this would correspond to a free stream Mach number of approximately 0.85. Additional studies are underway to optimize the low-speed high-lift components, depicted in Figure 16, for a lift coefficient of approximately 6.0. During the first phase of testing, the semi-span model will be fitted with a conventional leading edge slat. This will be replaced in subsequent testing with the leading edge blowing slot.



**Figure 15. Mach contours for the NASA TMA-0712 airfoil,  $M=0.78$ ,  $NPR=1.25$ .**

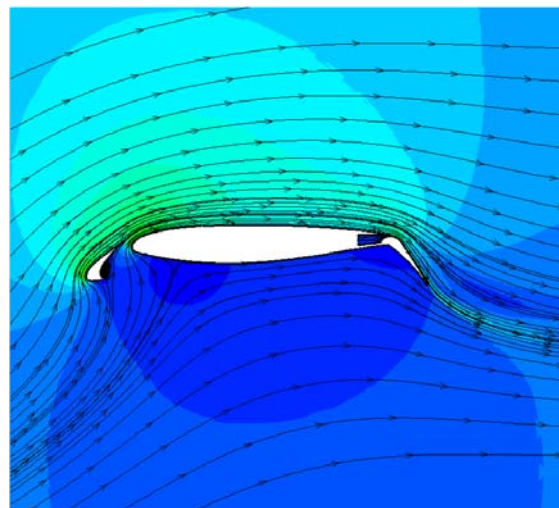


**Figure 16. Mach contours for the high-lift configuration for the NASA TMA-0712 airfoil,  $M=0.20$ .**

## Subsystem Case

A Hybrid Wing Body (HWB) model with blown flaps (see Figure 17) was tested in the NASA Langley 14-by-22-Foot Subsonic Tunnel (14x22) at low speeds ( $q = 30$  psf,  $M_\infty = 0.143$ ). The high-lift investigation was conducted as part of a 3-way collaboration between NASA LaRC, the Air Force Research Laboratory (AFRL), and the Northrop Grumman Systems Corporation (NGC) to advance state-of-the-art technologies for CESTOL aircraft. The enabling tools and technologies for CESTOL aircraft are dual use in that they are applicable for both military and civil missions. From the perspective of NASA's Subsonic Fixed Wing Project, the wind tunnel testing of the HWB model has provided unique databases to validate 3-D CFD tools for CESTOL efforts, particularly relating to the development of high-lift wings with advanced CC technologies.



**Figure 17. HWB model in the NASA Langley 14-by-22-Foot Subsonic Tunnel.**

The initial HWB test in the 14x22 used pressure sensitive paint (PSP) to complement pressure measurements from surface orifices. In addition, off-body flow field measurements were acquired with a 7-hole-probe rake survey system. Although only a reduced number of nozzle pressure ratios and geometrical settings (i.e., angles of attack of  $0^\circ$  and  $10^\circ$ , flap deflections of  $0^\circ$  and  $60^\circ$ , with and without the slat) were possible in the first tunnel entry, the experiment revealed several “lessons learned” issues and challenges associated with the PSP and 7-hole-probe measurements that need to be addressed for future tests.

PSP is an advanced pressure measurement technique that one would naturally consider for wind-tunnel testing of a full-span model because it can cover a substantial amount of surface area. PSP has demonstrated that it can provide reasonable visualization of surface pressure distributions globally. Nevertheless, the temperature gradients across the model due to a slow heat transfer associated with the jet plenums are a major challenge to overcome for the PSP technique. The plenums were preheated to the operational flow conditions prior to acquiring PSP data. While this reduced the temperature effect, the process was time consuming. One solution being developed for future testing is the use of a *biluminophore* PSP formulation to minimize the effect of temperature gradients.

The off-body measurements were obtained using standard 7-hole probe techniques. Eight 7-hole probes were mounted on the rake head connected to a probe positioning traverse system that was used to survey the wake of the left wing. All U, V, and W velocity components are in the tunnel coordinate system instead of model coordinate system. Figure 18 shows typical 7-hole probe results capturing complex and interesting flow features in the cross plane between the inboard flap edge and the outboard wing's trailing

edge. The two examples are the no blowing and blowing cases (NPR of 1.0 and 1.37, respectively) for the model with the slat installed, a flap deflection of  $60^\circ$ , and an AOA of  $10^\circ$ . The data are presented in terms of streamwise mean velocity (U) contours and velocity vectors in the Y-Z plane.

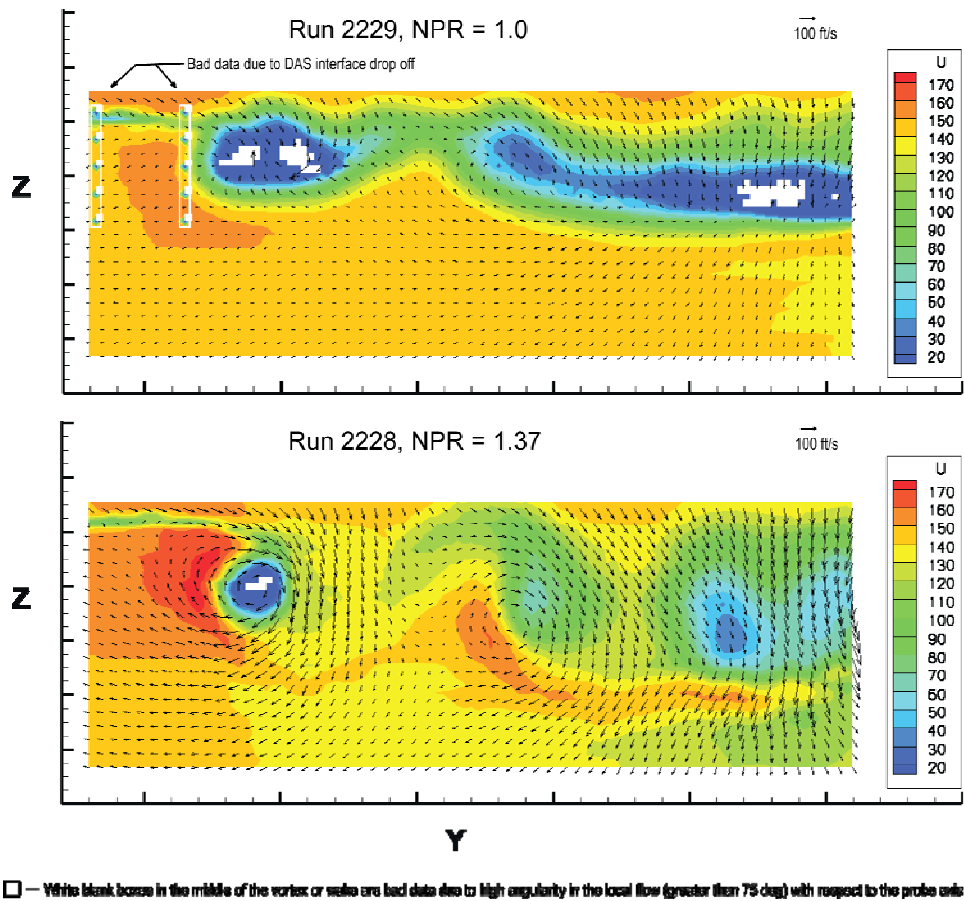


**Figure 18. U-velocity contours and velocity vectors in the Y-Z plane ( $M_\infty = 0.143$ ,  $60^\circ$  flap and slat on, AOA =  $10^\circ$ ).**

Two swirling regions downstream of the outboard flap edge and the inboard/outboard flap juncture are highlighted with velocity vectors for the blowing case (NPR = 1.37) shown in Figure 18. As expected, the increased lift associated with the  $60^\circ$  blown flap significantly enhanced the downwash velocity and the swirling. The stronger swirling is associated with a flap-edge-induced outboard vortex that has significantly more velocity deficit in its core than the weaker one downstream of the flap juncture. When viewing toward the upstream direction, the swirling motion is clockwise for both vortices. The outer edge of a third vortex with counter-clockwise rotation is caused by the inboard edge of the inboard flap and can be observed near the right edge of the plots.

White blanks in the middle of a vortex or wake for all cases indicate bad data (erroneous probe total pressure) due to high angularity in the local flows. Flows near the core of a wake vortex or near the off-body re-circulating regions often had flow angles greater than  $75^\circ$  with respect to the probe axis, which are outside the measuring capability of the 7-hole probes.

The 7-hole probe technique has demonstrated its capability of identifying complex and interesting flow features in the wake downstream, such as velocity-deficit and swirling-flow regions, for CFD code validation and for enhancing the understanding of the complex flow physics. In addition to the 7-hole probe measurements, a large field of view Particle Image Velocimetry (PIV) was used during the second wind tunnel entry in the wake of the model. The PIV system had some advantages such as non-intrusive and simultaneous acquisition of a plane of data. However, PIV data does not provide pressure information that can be correlated directly to the 7-hole probe data. It is also recognized that the particle density in the

strong vortex cores was too low to accurately resolve the velocities and that high tunnel temperature also influenced the particle density. Using both 7-hole probe and PIV data with uncertainty estimations is useful for CFD validation.

Documentation of the slot flow and boundary layer using a high resolution hot-wire survey is the best way to provide the blowing boundary conditions for CFD. In short, several different measurement techniques (i.e., force and moment, pressure orifices, PSP, 7-hole probes, PIV, hot-wires, Preston tubes, etc.) must be used in concert to provide a full database for CFD validation.

### **Complete System Case**

The advances realized through this CFD validation effort can be applied to integrated CC technologies applied to a CESTOL aircraft. Application of CC to a HWB concept, such as shown in Figure 19, will require the integration of several advanced systems. The development of a large-scale wind tunnel test or flight test for such an aircraft will require collaboration with industry and other government agencies.



**Figure 19. Sketch of a hybrid wing body configuration with circulation control technology applied to the outboard wing sections.**

### **Concluding Remarks**

This paper highlights on-going research efforts at NASA concerning circulation control that emphasize CFD validation and the creation of benchmark experimental databases to advance our knowledge base and prediction capabilities. The systematic CFD validation approach that is described in this report is consistent with NASA's foundational flow physics research for near-term conventional aircraft applications and longer-term hybrid wing-body configurations. The measurement and validation challenges for small-scale circulation control experiments are being pursued through the approach described in this paper. The circulation control examples shown in this paper highlight recent advances in CFD and experimental methods. These examples set the stage for developing wind tunnel databases related to supercirculation that will be required for CFD validation. The planned high-Reynolds-number experiments in NTF will provide a unique data set that will enable researchers to separate out the effects of the different blowing parameters so that they can better understand the complex physics of advanced circulation control applications. The outcomes of these efforts are expected to improve both experimental and CFD capabilities related to powered-lift and circulation control.

## References

- <sup>i</sup> Jones, G.S., Joslin, R.D., “Proceedings of the 2004 NASA/ONR Circulation Control Workshop”, NASA/CP-2005-213509, June 2005
- <sup>ii</sup> Swanson, R.C., Rumsey, C.L., Anders, S.G., “Progress Towards Computational Method for Circulation Control Airfoils”, AIAA 2005-0089, January 2005
- <sup>iii</sup> Slomski, J.F., Chang, P.A., Arunajatesan, S., “Large Eddy Simulation of a Circulation Control Airfoil”, AIAA-3011, June 2006
- <sup>iv</sup> *AIAA Guide to Verification and Validation*, AIAA G-077-1988
- <sup>v</sup> Roache, P.J., “*Verification and Validation in Computational Science and Engineering*,” Hermosa Publications, 1998
- <sup>vi</sup> Englar, R.J., Applegate, C.A., “Circulation control – A Bibliography of DTNSRDC Research and selected Outside References,” DTNSRDC-84/052, Sept 1984
- <sup>vii</sup> Wood, N., and Nielson, J. “Circulation Control Airfoils Past, Present, and Future,” AIAA Paper 850204, January, 1985
- <sup>viii</sup> Englar, R.J., Circulation control Pneumatic Aerodynamics: blown force and Moment Augmentation and Modifications; Past, Present, & Future”, AIAA 2000-2541, June 2000
- <sup>ix</sup> Loth, J.L., J.D. Fanucci and S.C. Roberts, “Flight Performance of a Circulation Control STOL Aircraft,” AIAA Paper 74-994, April 1974; AIAA Journal of Aircraft, Vol. 13, No.3, pp. 169-173, March 1976
- <sup>x</sup> Englar, R.J., “Development of the A-6/Circulation Control Wing Flight Demonstrator Configuration,” DTNSRDC Report ASED-79/01, January 1979
- <sup>xi</sup> Pugliese, A.J. (Grumman Aerospace Corporation) and R. J. Englar (DTNSRDC), "Flight Testing the Circulation Control Wing," AIAA Paper No. 79-1791 presented at the *AIAA Aircraft Systems and Technology Meeting*, August, 1979
- <sup>xii</sup> Zuk, J., Callaway, R.K., and Wardwell, D.A., “Adaptive Air Transportation System – A Catalyst for Change”, AIAA 2002-5956, November 2002
- <sup>xiii</sup> Lilley, G.M., “Circulation Control for Quiet Commercial Aircraft”, AIAA 2006-2842, June 2006
- <sup>xiv</sup> Federal Aviation Administration, “Aviation System Performance Metrics, (ASPM),” July 2007
- <sup>xv</sup> Burleson, C., “Aviation and the Environment – Managing the Challenge of Growth”, NASA Fundamental Aeronautics Meeting, New Orleans, October 30, 2007
- <sup>xvi</sup> Callaway, R.K.; Wardwell, D.A.; Zuk, J., “Development of a System Engineering Process for an ESTOL Transport Planning Activity”, AIAA 2003-6856, November 2003
- <sup>xvii</sup> Zuk, J. and Wardwell, D.A., “Summary of NASA’s Extreme Short Take-Off and Landing (ESTOL) Vehicle Sector Activities.” NASA/CP-2005-013145, pp. 1-14
- <sup>xviii</sup> Burnside, J.J., Storms, B.L., Horne, W.C., and Hange, C.E., “C-17 Noise Footprint Measurements Using a Low-Cost Distributed Data Acquisition System”, AIAA 2007-1399, January 2007
- <sup>xix</sup> Couluris, G.J., Hange, C.E., Wardwell, D.A., “A Potential Impact Analysis of ESTOL Aircraft on Newark Airport Operations”, AIAA 2007-6700, August 2007
- <sup>xx</sup> Rich, P., McKinley, R.J., Jones, G.S., “Circulation Control in NASA’s Vehicle Systems”, NASA CP-205-213509 (part 1), June 2005
- <sup>xxi</sup> Callaway, R.K., Wardwell, D.A, Zuk, J., “Development of a System Engineering Process for an ESTOL Transport Planning Activity”, AIAA 2003-6856, November 2003
- <sup>xxii</sup> Ball, T., Turner, S. and Marshall, D., “Short Takeoff Performance using Circulation Control”, AIAA 2008-174, January 2008
- <sup>xxiii</sup> Bobbitt, P.J., Margason, R., “Analysis of the Take-Off and Landing of a Powered-Lift Aircraft,”, AIAA 2007-1256, January 2007
- <sup>xxiv</sup> Menter, F.R., “Two-Equation Eddy-Viscosity Turbulence Models for Engineering Applications,” AIAA Journal, Vol. 32, No. 8, 1994, pp. 1598—1605.
- <sup>xxv</sup> Shur, M.L., Strelets, M.K., Travin, A.K., and Spalart, P.R., “Turbulence Modeling in Rotating and Curved Channels: Assessing the Spalart-Shur Correction,” AIAA Journal, Vol. 38, No. 5, 2000, pp. 784-792
- <sup>xxvi</sup> Jones, G.S., Viken, S.A., Washburn, A.E., Jenkins, L.N., & Cagle, C.M., “An Active Flow Circulation Controlled Flap Concept for General Aviation Applications”, AIAA 2002-3157, June 2002

---

<sup>xxvii</sup> Jones, G.S., Yao, C., Allan, B.G., “Experimental Investigation of a 2-D Supercritical Circulation-Control airfoil Using Particle Image Velocimetry, AIAA-2006-3009, June 2006

<sup>xxviii</sup> “*Assessing Experimental Uncertainty*-Supplement to AIAA S-071A-1999,” AIAA G-045-2003

<sup>xxix</sup> Coleman, H.W., Steele, W.G., “*Experimentation and Uncertainty Analysis for Engineers* (2<sup>nd</sup> Edition)”, John Wiley & Sons Publication, 1999

<sup>xxx</sup> Novak, C.J., Cornelius, K.C., and Roads, R. K., “Experimental Investigations of the Circular Wall Jet on a Circulation Control Airfoil,” AIAA Paper 87-0155, 1987

<sup>xxxi</sup> DeLaMontanya, J.B., Marshall, D.D., “Circulation Control and Its Application to Extreme Short Take-Off and Landing Vehicles”, AIAA 2007-1404, January 2007